Bull. Soc. R. Sci. Liège, 2024, **93**(2), 146–154 *Peer-reviewed conference paper*
doi:10.25518/0037-9565.11630

Coronal Modulation in the Ultra-fast Rotator LO Peg

Gurpreet SINGH[1,2,*], Jeewan Chandra PANDEY[1] and Umesh YADAVA[2]

[1] Aryabhatta Research Institute of observational sciencES, Manora Peak, Nainital, 263001, India
[2] Deen Dayal Upadhyaya Gorakhpur University, Gorakhpur, 273009, India
[*] Corresponding author: gurpreet@aries.res.in

Paper presented at the 3rd BINA Workshop on "Scientific Potential of the Indo-Belgian Cooperation", held at the Graphic Era Hill University, Bhimtal (India), 22nd–24th March 2023.

Abstract

We present coronal imaging of the ultra-fast rotator, LO Peg, using the X-ray observations from XMM-Newton. The X-ray light curves show one strong flare at the end of observation, as reported in an earlier study. On removal of flaring events, the quiescent state light curve shows rotational modulations, which are modelled using a maximum likelihood model. The results obtained from modelling show that the corona of LO Peg is not uniform. Active regions are concentrated around two longitudes, where one active region appears to be compact. The large coronal area that covers almost 60 degrees along longitude from the poles to the equator does not consist of active regions.

Keywords: Stellar activity — Stellar Coronae — X-ray star — X-ray astronomy — Stellar imaging

1. Introduction

The light curves of late-type active stars exhibit a wide range of temporal variability across the electromagnetic spectrum, spanning from minutes to decades. This variability can be categorized into short-term variability (STV) and long-term variability (LTV), which are manifestations of different magnetic activities. STV, lasting from a few minutes to a few days, is primarily attributed to flaring activity and rotational modulation caused by inhomogeneities in the corona. Extensive studies and modelling of STVs due to flares have been conducted, shedding light on the extreme physical conditions of solar-type stars (e.g., Haisch et al., 1991; Reale, 2007; Pandey and Singh, 2008, 2012). Several techniques have been employed to extract information from periodic STVs resulting from rotational modulations of active regions in stellar atmospheres. These include Doppler imaging using X-ray data (Brickhouse et al., 2001), extrapolation of surface magnetic maps (Hussain et al., 2007; Johnstone et al., 2010; Cohen et al., 2010, etc.), and light curve inversion techniques (Siarkowski, 1992; Siarkowski et al., 1996; Drake et al., 2014; Singh and Pandey, 2022). However, each technique has its limitations. Doppler imaging of X-ray data requires high-spectral resolution, often unavailable due to

instrumental and observing constraints. Inferring coronal structures based on magnetic surface maps necessitates simultaneous observations in optical and X-ray bands. Light-curve inversion techniques (LCITs) pose a mathematically ill-posed problem, extracting 3-D information from 1-D time-series data. Despite these challenges and reasonable inputs, the LCITs have gained popularity due to the increasing availability of time-series data.

This paper presents the results obtained by an X-ray LCIT for an ultra-fast rotator (UFR) LO Peg. LO Peg is a K5-8V type UFR with a rotation period of 0.423 d (Karmakar et al., 2016). The active nature of LO Peg in optical and X-ray bands has been studied in detail in the past (e.g., Jetsu et al., 1994; Eibe et al., 1999; Pandey et al., 2005, 2009; Karmakar et al., 2016). The Doppler imaging of LO Peg has shown high-latitude spots (Lister et al., 1999; Piluso et al., 2008). Based on long-term optical data, Karmakar et al. (2016) has shown an excess of X-ray emission in spotted regions where the spotted regions can cover the stellar surface from 9 to 26%. They have also found evidence of the presence of the flip-flop-like phenomenon.

We organise our paper as follows: Section 2 shows observations and data reduction, and Section 3 presents the analysis and results. The coronal imaging method is described in Section 4, and application to this method is shown in Section 5. We conclude in Section 6 with the key findings from this research.

2. Observations and Data Reduction

The XMM-Newton observatory observed LO Peg for 42 ks on 30 November 2014. XMM-Newton is equipped with three X-ray telescopes featuring five detectors: 2 MOS (Turner et al., 2001), 1 PN (Strüder et al., 2001), and 2 RGS (den Herder et al., 2001). These detectors cover an energy range of 0.15–15 keV. In addition to the X-ray detectors, XMM-Newton also includes an optical monitor payload (OM; Mason et al., 2001), enabling simultaneous observations in the UV and optical bands.

The raw data obtained from the observation was processed using the Science Analysis System (SAS) v18.0.0 software (https://www.cosmos.esa.int/web/xmm-newton/sas). Standard procedures provided by the software were applied to generate the science products. The source light curves were created by considering the X-ray counts within a circular region of radius 42″. Similarly, background light curves were generated from source-free regions in the same CCD, utilizing an extracted area similar to the source. Subsequently, the background subtraction and detector response effects were corrected using the EPICLCCORR task.

3. Analysis and Results

The background corrected light curves for LO Peg are shown in Fig. 1 in three energy bands, namely a broad band which covers 0.3–10.0 keV energy range, a soft band with an energy band of 0.3–2.0 keV, and a hard band containing photons of energy 2.0–10.0 keV. The light curves in all three bands show one standard flare-like time profile marked as blue-shaded regions in Fig. 1. This detected flare also shows temperature variations indicated by the hardness ratio (HR) plot

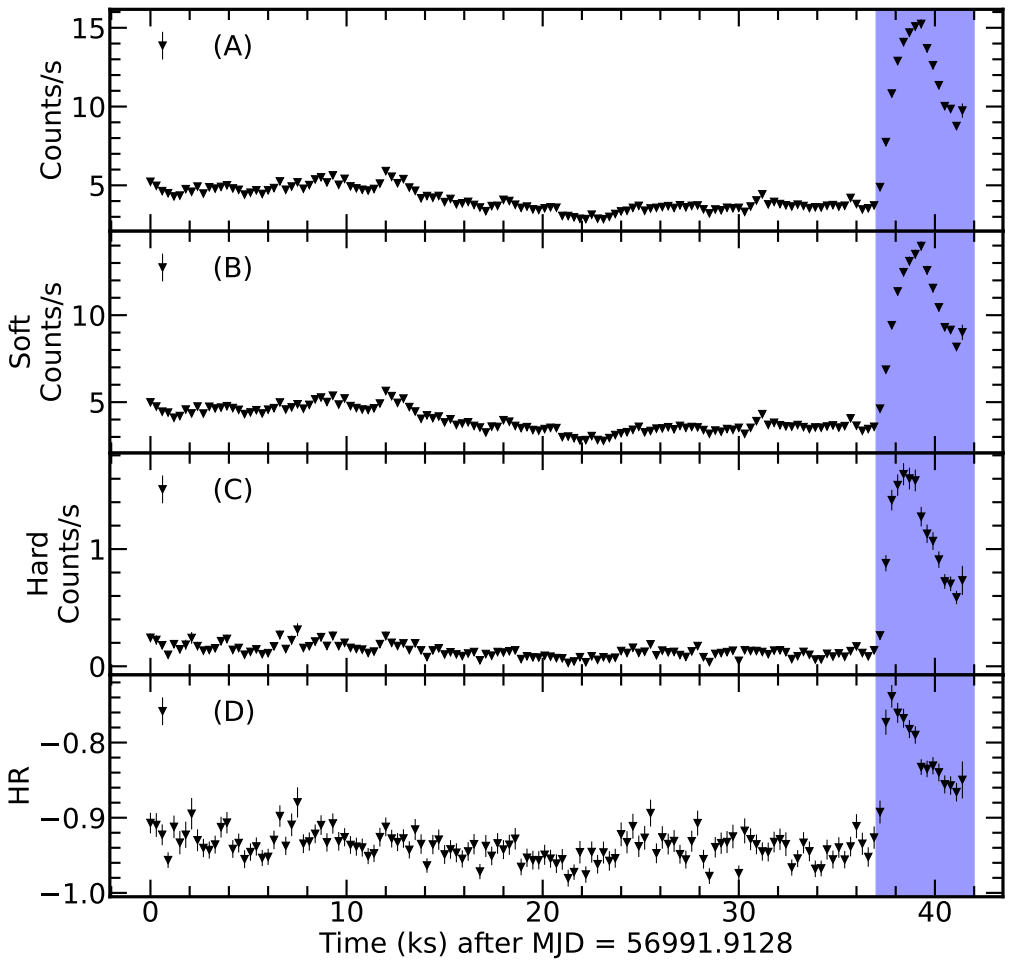

Figure 1: EPIC-PN X-ray light curve of LO Peg with a time bin size of 300 sec. Panel (A) shows an X-ray light curve in 0.3–10.0 keV, with panels (B) and (C) showing soft (0.3–2.0 keV) and hard (2.0–10.0 keV) bands. The lowermost panel (D) shows the hardness ratio (HR). The blue-shaded regions correspond to flaring episodes.

and shown in the lowermost panel of Fig. 1. The HR is defined as Hard-Soft/Hard+Soft, where Hard and Soft are count rates in 2.0–10.0 keV and 0.3–2.0 keV energy bands, respectively. From the HR plot, the mean value of HR ~ -0.9 indicates that LO Peg's corona is predominantly populated by low-energy photons with energy less than 2 keV. The ratio of median values of soft counts and total band counts shows that photons with energy less than 2 keV contribute 96% of the total band energy spectrum. Thus, the quiescent corona of LO Peg predominantly consists of plasma with a temperature of less than 2 keV.

If we exclude the flaring part from the light curve, the quiescent state light curve appears variable in the time scale of its rotation period. Therefore, we have phase-folded the quiescent light curve to check for the rotationally modulated signal with ephemeris given by Dal and Tas

(2003) with the rotational period obtained by Karmakar et al. (2016). The phase folded light curve is shown in Fig. 2(a), and rotational modulation was found to be present with an amplitude of $> 20\%$ about the mean value. Estimating rotational modulation from a single rotation period is prone to small-scale fluctuations. However, it is essential to note that the rotational modulation for the same observation was previously reported by Lalitha et al. (2017). Additionally, to mitigate the influence of short-term stochastic variability in the folded light curve, we have phase-folded the light curve into 30 bins, corresponding to a 1.22 ks time interval. This process allows for averaging stochastic variability caused by micro- and nano-flares, emphasising only the large-scale variations. The phase-folded quiescent light curve was modelled using a maximum likelihood algorithm, which is discussed briefly as follows.

4. Coronal Imaging: Model

We have assumed that the coronal plasma is optically thin and rotates rigidly, and the variability seen in quiescent emission is mainly due to the active regions in the corona, which are being eclipsed by the cylindrical shadow cast by the stellar photosphere during observation. Further, we divide the volume around the star into a total of B cubical boxes, each associated with an emission density f. The boxes around the star are distributed up to a height h above the stellar photosphere. The number of photons emitted by a cubical box (b) follows a Poisson distribution with a mean value of $f(b)$, which is given as

$$P(n(b) = k) = e^{-f(b)} \frac{f(b)^k}{k!}, \quad k = 0, 1, 2, \ldots$$

We aim to find each box's $f(b)$. For instance, there are 'N' observations during one rotational phase, and then different parts of the star become visible with the progressing rotational phase. As the plasma is assumed to be optically thin at any given phase value (ϕ), the total emission can be calculated by adding all the visible cubical boxes. To calculate which box is visible at any given phase, we assume that the only occulter to the corona is the stellar photosphere, which casts a cylindrical shadow on the corona. We calculate an occultation matrix $M(b, \phi)$ consisting of weights assigned to each box equal to 1 if visible and 0 if occulted. So, the total emission at any given phase is given by

$$F(\phi) = \sum_b f(b) M(b, \phi) db$$

Due to the inclination angle of the star, some boxes are never seen during the whole observation, and some boxes are always visible. The boxes not seen should be excluded from the solution grid as they do not contribute to any of the variability seen in the light curves if we assume the emission from each box is stable during the observation. The conditional probability of observing counts $F_o(\phi_i)$ at phase ϕ_i with known emissions in each box $f(b)$ and occultation matrix $M(b, \phi_i)$ can be written as

$$P_i(F_o(\phi_i)|f, M(\phi_i)) = \mathrm{e}^{-\lambda} \frac{\lambda^{F_o(\phi_i)}}{F_o(\phi_i)!}, \quad \lambda = \sum_b f(b) M(b, \phi_i) db$$

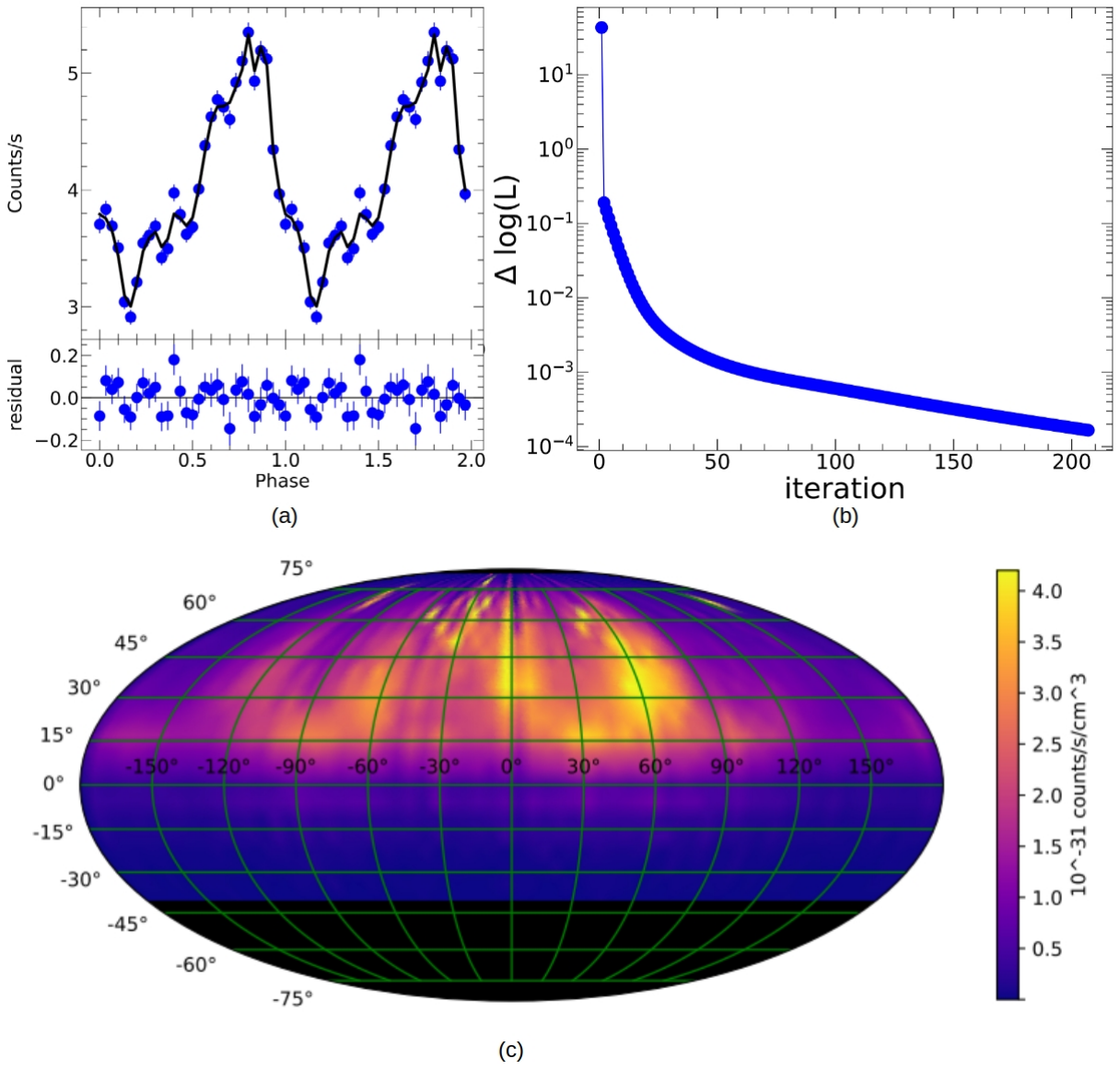

Figure 2: Results from coronal imaging of LO Peg: (a) observed and the best fit modelled X-ray light curves, (b) $\Delta\log(L)$ vs iteration showing likelihood is strictly increasing in each iteration, and (c) projected coronal image of LO Peg. Here, the colour bar shows emission values at each latitude and longitude. The black-shaded regions correspond to latitudes which do not contribute to rotational modulation.

The log-likelihood function can be written as

$$\log(L) = \sum_i \log(P_i) = \sum_i \big(-\lambda + F_o(\phi_i)\log(\lambda) - \log(\Gamma(F_o(\phi_i)+1)) \big) \tag{1}$$

We now describe an iterative scheme that maximises the above-said setup's likelihood.

$$f^{n+1}(b) = f^n(b) \times \frac{\sum_i \frac{F_o(\phi_i)}{\sum_b f^n(b) M(b,\phi) db} M(b,\phi_i)}{\sum_i M(b,\phi_i)} \tag{2}$$

The above equation updates the old estimate for emission in box b by considering the previous value of f at point b, scaling it based on the ratio of $F_o(\phi_i)$ to the weighted average of F_o for the all b boxes, and then normalising it by the sum of the weighting function M for all phases ϕ_i.

5. Coronal Imaging of LO Peg

For the current solution, we have used a resolution of $0.05 \times 0.05 \times 0.05\,R_\odot$, with an inclination angle fixed to 45° and radius of $0.72\,R_\odot$ for LO Peg (Pandey et al., 2005) with coronal height up to $1\,R_*$. We start with a uniform emission in each box for the first iteration step, which is then updated according to Eqn. (2). At each iteration step, we also calculate the log-likelihood as per Eqn. (1). The iteration was stopped when observed, and modelled count rates were fitted well as per the standard χ^2 scheme. The coronal image and modelled light curves are shown in Fig. 2. In the same Figure, we plot the log-likelihood function's positive difference, showing that each iteration strictly increases the likelihood.

From Fig. 2(c), the corona of LO Peg shows active regions are not uniformly distributed across the corona. Active regions are located between the longitudes -120° to $+120^\circ$ with brighter active regions around $+60^\circ$. Around -90 to -60° longitude, the corona has a fainter active region. Similar longitudinal distribution in the photosphere is also reported for LO Peg during the year 2014–2015 (Savanov et al., 2016). Active regions appear to be absent around the longitudes $+120^\circ$ to $+180^\circ$, which may be an indication of a coronal hole.

6. Conclusions

We have found that the quiescent emission of LO Peg is not constant but shows rotational modulation with an amplitude of $> 20\%$ about the mean value. This modulation is modelled by a maximum-likelihood method, revealing that the corona of LO Peg is not uniform but is concentrated towards two longitudes. Active regions are concentrated in the two different longitudes.

Acknowledgments

This work is based on observations obtained with XMM-Newton, an ESA science mission with instruments and contributions directly funded by ESA Member States and NASA.

Further Information

Authors' ORCID identifiers

0009-0002-6580-3931 (Gurpreet SINGH)
0000-0002-4331-1867 (Jeewan Chandra PANDEY)
0000-0002-9127-532X (Umesh YADAVA)

Author contributions

All authors contributed significantly to the work presented in this paper.

Conflicts of interest

The authors declare no conflict of interest.

References

Brickhouse, N. S., Dupree, A. K. and Young, P. R. (2001) X-ray Doppler imaging of 44i Bootis with *Chandra*. ApJ, 562(1), L75–L78. https://doi.org/10.1086/338121.

Cohen, O., Drake, J. J., Kashyap, V. L., Hussain, G. A. J. and Gombosi, T. I. (2010) The coronal structure of AB Doradus. ApJ, 721(1), 80–89. https://doi.org/10.1088/0004-637X/721/1/80.

Dal, H. A. and Tas, G. (2003) New photoelectric photometry of the young star LO Pegasi. IBVS, 5390, 1.

den Herder, J. W., Brinkman, A. C., Kahn, S. M., Branduardi-Raymont, G., Thomsen, K., Aarts, H., Audard, M., Bixler, J. V., den Boggende, A. J., Cottam, J., Decker, T., Dubbeldam, L., Erd, C., Goulooze, H., Güdel, M., Guttridge, P., Hailey, C. J., Janabi, K. A., Kaastra, J. S., de Korte, P. A. J., van Leeuwen, B. J., Mauche, C., McCalden, A. J., Mewe, R., Naber, A., Paerels, F. B., Peterson, J. R., Rasmussen, A. P., Rees, K., Sakelliou, I., Sako, M., Spodek, J., Stern, M., Tamura, T., Tandy, J., de Vries, C. P., Welch, S. and Zehnder, A. (2001) The reflection grating spectrometer on board *XMM-Newton*. A&A, 365, L7–L17. https://doi.org/10.1051/0004-6361:20000058.

Drake, J. J., Ratzlaff, P., Kashyap, V., Huenemoerder, D. P., Wargelin, B. J. and Pease, D. O. (2014) A 33 yr constancy of the X-ray coronae of AR= Lac and eclipse diagnosis of scale height. ApJ, 783(1), 2. https://doi.org/10.1088/0004-637X/783/1/2.

Eibe, M. T., Byrne, P. B., Jeffries, R. D. and Gunn, A. G. (1999) Evidence for large–scale, global mass inflow and flaring on the late–type fast rotator BD+22 deg 4409. A&A, 341, 527–538.

Haisch, B., Strong, K. T. and Rodono, M. (1991) Flares on the Sun and other stars. ARA&A, 29, 275–324. https://doi.org/10.1146/annurev.aa.29.090191.001423.

Hussain, G. A. J., Jardine, M., Donati, J. F., Brickhouse, N. S., Dunstone, N. J., Wood, K., Dupree, A. K., Collier Cameron, A. and Favata, F. (2007) The coronal structure of AB Doradus determined from contemporaneous Doppler imaging and X-ray spectroscopy. MNRAS, 377(4), 1488–1502. https://doi.org/10.1111/j.1365-2966.2007.11692.x.

Jetsu, L., Tuominen, I., Grankin, K. N., Mel'Nikov, S. Y. and Schevchenko, V. S. (1994) New "flip–flop" of FK Comae Berenices. A&A, 282, L9–L12.

Johnstone, C., Jardine, M. and Mackay, D. H. (2010) Modelling stellar coronae from surface magnetograms: the role of missing magnetic flux. MNRAS, 404(1), 101–109. https://doi.org/10.1111/j.1365-2966.2010.16298.x.

Karmakar, S., Pandey, J. C., Savanov, I. S., Taş, G., Pandey, S. B., Misra, K., Joshi, S., Dmitrienko, E. S., Sakamoto, T., Gehrels, N. and Okajima, T. (2016) LO Peg: surface differential rotation, flares, and spot-topographic evolution. MNRAS, 459(3), 3112–3129. https://doi.org/10.1093/mnras/stw855.

Lalitha, S., Schmitt, J. H. M. M. and Singh, K. P. (2017) Structure and variability in the corona of the ultrafast rotator LO Pegasi. A&A, 602, A26. https://doi.org/10.1051/0004-6361/201629482.

Lister, T. A., Collier Cameron, A. and Bartus, J. (1999) Doppler imaging of BD+22 deg4409 (LO Peg) using least-squares deconvolution. MNRAS, 307(3), 685–694. https://doi.org/10.1046/j.1365-8711.1999.02662.x.

Mason, K. O., Breeveld, A., Much, R., Carter, M., Cordova, F. A., Cropper, M. S., Fordham, J., Huckle, H., Ho, C., Kawakami, H., Kennea, J., Kennedy, T., Mittaz, J., Pandel, D., Priedhorsky, W. C., Sasseen, T., Shirey, R., Smith, P. and Vreux, J. M. (2001) The *XMM-Newton* optical/UV monitor telescope. A&A, 365, L36–L44. https://doi.org/10.1051/0004-6361:20000044.

Pandey, J. C., Medhi, B. J., Sagar, R. and Pandey, A. K. (2009) LO Pegasi: an investigation of multiband optical polarization. MNRAS, 396(2), 1004–1011. https://doi.org/10.1111/j.1365-2966.2009.14762.x.

Pandey, J. C. and Singh, K. P. (2008) A study of X-ray flares – I. Active late–type dwarfs. MNRAS, 387(4), 1627–1648. https://doi.org/10.1111/j.1365-2966.2008.13342.x.

Pandey, J. C. and Singh, K. P. (2012) A study of X-ray flares – II. RS CVn–type binaries. MNRAS, 419(2), 1219–1237. https://doi.org/10.1111/j.1365-2966.2011.19776.x.

Pandey, J. C., Singh, K. P., Drake, S. A. and Sagar, R. (2005) Optical and X-ray studies of chromospherically active stars: FR Cancri, HD 95559, and LO pegasi. AJ, 130(3), 1231–1246. https://doi.org/10.1086/432539.

Piluso, N., Lanza, A. F., Pagano, I., Lanzafame, A. C. and Donati, J. F. (2008) Doppler imaging of the young late-type star LO pegasi (BD+22°4409) in 2003 September. MNRAS, 387(1), 237–246. https://doi.org/10.1111/j.1365-2966.2008.13153.x.

Reale, F. (2007) Diagnostics of stellar flares from X-ray observations: from the decay to the rise phase. A&A, 471(1), 271–279. https://doi.org/10.1051/0004-6361:20077223.

Savanov, I. S., Puzin, V. I., Dmitrienko, E. S., Karpov, S. V., Beskin, G. M., Biryukov, A. V., Bondar, S. F., Ivano, E. A., Katkova, E. V., Orekhova, N., Perkov, A. V., Sasyuk, V. V., Romanyuk, I. I., Semenko, E. A., Kudryavtsev, D., Karmakar, S., Pandey, J. C., Pandey, S. B., Joshi, S. and Misra, K. (2016) Photometric observations of LO Peg in 2014–2015. AcA, 66(3), 381–390.

Siarkowski, M. (1992) Three-dimensional deconvolution of X-ray emission from AR Lac. MNRAS, 259, 453–456. https://doi.org/10.1093/mnras/259.3.453.

Siarkowski, M., Pres, P., Drake, S. A., White, N. E. and Singh, K. P. (1996) Corona(e) of AR Lacertae. II. The spatial structure. ApJ, 473, 470. https://doi.org/10.1086/178159.

Singh, G. and Pandey, J. C. (2022) An X-ray study of coronally connected active eclipsing binaries. ApJ, 934(1), 20. https://doi.org/10.3847/1538-4357/ac7716.

Strüder, L., Briel, U., Dennerl, K., Hartmann, R., Kendziorra, E., Meidinger, N., Pfeffermann, E., Reppin, C., Aschenbach, B., Bornemann, W., Bräuninger, H., Burkert, W., Elender, M., Freyberg, M., Haberl, F., Hartner, G., Heuschmann, F., Hippmann, H., Kastelic, E., Kemmer, S., Kettenring, G., Kink, W., Krause, N., Müller, S., Oppitz, A., Pietsch, W., Popp, M., Predehl, P., Read, A., Stephan, K. H., Stötter, D., Trümper, J., Holl, P., Kemmer, J., Soltau, H., Stötter, R., Weber, U., Weichert, U., von Zanthier, C., Carathanassis, D., Lutz, G., Richter, R. H., Solc, P., Böttcher, H., Kuster, M., Staubert, R., Abbey, A., Holland, A., Turner, M., Balasini, M., Bignami, G. F., La Palombara, N., Villa, G., Buttler, W., Gianini, F., Lainé, R., Lumb, D. and Dhez, P. (2001) The European Photon Imaging Camera on *XMM-Newton*: The pn-CCD camera. A&A, 365, L18–L26. https://doi.org/10.1051/0004-6361:20000066.

Turner, M. J. L., Abbey, A., Arnaud, M., Balasini, M., Barbera, M., Belsole, E., Bennie, P. J., Bernard, J. P., Bignami, G. F., Boer, M., Briel, U., Butler, I., Cara, C., Chabaud, C., Cole, R., Collura, A., Conte, M., Cros, A., Denby, M., Dhez, P., Di Coco, G., Dowson, J., Ferrando, P., Ghizzardi, S., Gianotti, F., Goodall, C. V., Gretton, L., Griffiths, R. G., Hainaut, O., Hochedez, J. F., Holland, A. D., Jourdain, E., Kendziorra, E., Lagostina, A., Laine, R., La Palombara, N., Lortholary, M., Lumb, D., Marty, P., Molendi, S., Pigot, C., Poindron, E., Pounds, K. A., Reeves, J. N., Reppin, C., Rothenflug, R., Salvetat, P., Sauvageot, J. L., Schmitt, D., Sembay, S., Short, A. D. T., Spragg, J., Stephen, J., Strüder, L., Tiengo, A., Trifoglio, M., Trümper, J., Vercellone, S., Vigroux, L., Villa, G., Ward, M. J., Whitehead, S. and Zonca, E. (2001) The European Photon Imaging Camera on *XMM-Newton*: The MOS cameras. A&A, 365, L27–L35. https://doi.org/10.1051/0004-6361:20000087.